Coupling of protonation, reduction and conformational change in azurin from *Pseudomonas aeruginosa* investigated with free energy measures of cooperativity

R. Thomas Ullmann and G. Matthias Ullmann*

Structural Biology / Bioinformatics, University of Bayreuth,
Universitätsstr. 30, BGI, 95447 Bayreuth, Germany

* Email: Matthias.Ullmann@uni-bayreuth.de

Submitted

Supporting Information

Contents

A Supporting figures, plots and tables

Additional plots and tables of simulation results give a more detailed overview of the results presented in the main text.

A.1 Macroscopic binding behavior

Table S1 contains the intrinsic energies of all macroscopic binding states of PaAz. The intrinsic energies of the macroscopic binding states have a clear relation to the electrochemical potential of the corresponding receptor species in solution.[1] Macroscopic binding properties of PaAz can be expressed in terms of these intrinsic energies.[1] This formulation allows to discern the influence of intrinsic receptor properties and ligand chemical potentials on the binding behavior of the system.

The intrinsic energy of macrostate a is calculated from its partition function $\mathcal{Z}_a$ as

$$E_a^{\mathrm{int,macro}} = -\beta^{-1} \ln \mathcal{Z}_a + \sum_m^{\mathfrak{L}} \nu_{a,m} \bar{\mu}_m \tag{S1}$$

where $\mathfrak{L}$ is the number of ligand types and the stoichiometric coefficient $\nu_{a,m}$ indicates the number of ligands of type m bound in macrostate a. $\bar{\mu}_m$ is the electrochemical potential of ligand type m in the surrounding solution. The partition function of the macrostate is given by

$$\mathcal{Z}_a = \sum_{\boldsymbol{n}}^{\mathfrak{N}_a} \exp\left[-\beta E_{\boldsymbol{n}}^{\mathrm{micro}}\right] \tag{S2}$$

where the sum runs over all $\mathfrak{N}_i$ microstates $\boldsymbol{n}$ that form the macrostate a. The microstate energy is given by Eq. (1) of the main text. Note that the macroscopic intrinsic energies are independent of the ligand chemical potentials, as can be seen from comparison of Eq. (1) and Eq. (S1).

The partition functions were computed numerically with Wang-Landau MC as described in reference 1. Simulation data for different ligand chemical potential combinations was averaged. For the averaging, we used for each macrostate only those simulations in which the macrostate was significantly populated to ensure proper statistical convergence of the corresponding histogram.[1] The partition function of PaAz in terms of macroscopic intrinsic energies is given by

$$\mathcal{Z} = \sum_a^{\mathfrak{N}^{\mathrm{macro}}} \exp\left[-\beta\left(E_a^{\mathrm{int,macro}} - \sum_m^{\mathfrak{L}} \nu_{a,m}\bar{\mu}_m\right)\right] \tag{S3}$$

where the sum runs over all $\mathfrak{N}^{\mathrm{macro}}$ binding macrostates a. The equilibrium occupation probability p_a of binding macrostate a is given by

$$p_a = \frac{\mathcal{Z}_a}{\mathcal{Z}} \tag{S4}$$

The free energy difference between two binding macrostates i, j is given by

$$\Delta G_{a\to b} = -\beta^{-1} \ln \frac{\mathcal{Z}_b}{\mathcal{Z}_a} \tag{S5}$$

Inserting Eq. (S2) and collecting terms yields the following expression for the free energy difference between two binding macrostates as a function of their intrinsic energies and the ligand chemical potentials

$$\Delta G_{a\to b} = E_b^{\mathrm{int,macro}} - E_a^{\mathrm{int,macro}} - \sum_m^{\mathfrak{L}} \left[\left(\nu_{b,m} - \nu_{a,m} \right) \bar{\mu}_m \right] \tag{S6}$$

where the difference in the intrinsic energies accounts for internal changes within PaAz and the sum over the ligand chemical potentials accounts for the cost of exchanging ligands with the surrounding solution. Note that the relative intrinsic energies for the macroscopic reduction and protonation states with respect to the fully unbound macrostate in Table S1 are identical to the corresponding standard binding free energies.

$$G_{\mathrm{unbound}\to b}^{\circ,\mathrm{bind,macro}} = E_b^{\mathrm{int,macro}} - E_{\mathrm{unbound}}^{\mathrm{int,macro}} - \sum_m^{\mathfrak{L}} \nu_{b,m} \mu_m^{\circ} \tag{S7}$$

This is, because the standard chemical potentials μ° of the electron and the proton in solution are equal to zero by definition.[1]

Figure S1 shows plots of the macroscopic binding probabilities in dependence on the pH value and the reduction potential of the solution. Figure S2 shows the number of effectively populated macroscopic reduction and protonation states plotted as functions of the pH value and the reduction potential of the solution. The effectively populated number of binding macrostates can be calculated from the Süßmann entropy.[2,3] Figure S3 shows the free energies for all stepwise macroscopic binding reactions of PaAz as functions of the pH value and the reduction potential of the solution.

Protons bound	Intrinsic energy in kcal/mol		
	oxidized	reduced	reduced − oxidized
0	0.0	1.6	1.6
1	-42.7	-45.0	-2.3
2	-69.8	-72.5	-2.7
3	-95.1	-98.0	-2.9
4	-117.5	-120.4	-3.0
5	-138.1	-141.2	-3.2
6	-157.9	-161.2	-3.3
7	-177.3	-180.7	-3.4
8	-196.3	-199.8	-3.5
9	-214.9	-218.6	-3.7
10	-233.1	-236.9	-3.8
11	-251.0	-254.9	-3.9
12	-268.5	-272.6	-4.1
13	-285.5	-289.8	-4.3
14	-302.1	-306.6	-4.5
15	-318.1	-322.7	-4.7
16	-333.4	-338.2	-4.8
17	-344.8	-350.0	-5.2
18	-355.3	-361.1	-5.7
19	-364.9	-371.6	-6.7
20	-373.5	-381.2	-7.7
21	-381.0	-389.0	-8.0
22	-388.1	-396.3	-8.2
23	-394.7	-403.1	-8.4
24	-401.0	-409.5	-8.5
25	-407.0	-415.7	-8.7
26	-412.7	-421.5	-8.8
27	-418.1	-427.1	-8.9
28	-423.3	-432.4	-9.1
29	-428.2	-437.3	-9.2
30	-432.7	-442.0	-9.3
31	-436.9	-446.4	-9.4
32	-440.7	-450.3	-9.6
33	-444.0	-453.7	-9.7
34	-445.0	-455.3	-10.3
35	-444.3	-455.0	-10.7

Table S1: Intrinsic energies of macroscopic protonation states for oxidized and reduced PaAz and intrinsic energy shift upon reduction. For clarity, the intrinsic energies are expressed relative to the oxidized, fully deprotonated macrostate.

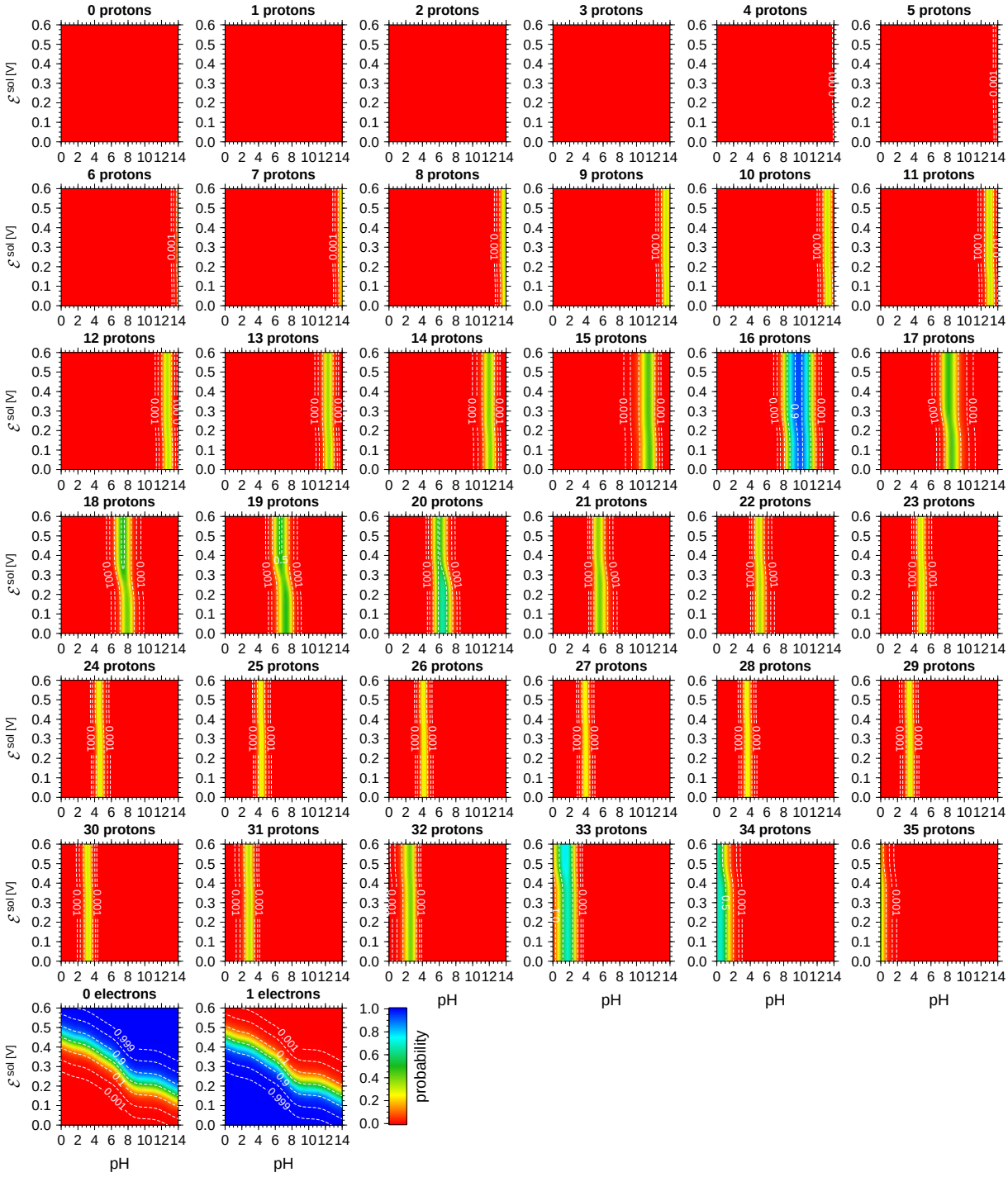

Figure S1: The occupation probabilities of macroscopic protonation and reduction states of PaAz as functions of the pH value and reduction potential of the solution. The number of protons or electrons bound is indicated by the curve labels. The probability is color coded (see color bar) and indicated by the contour values.

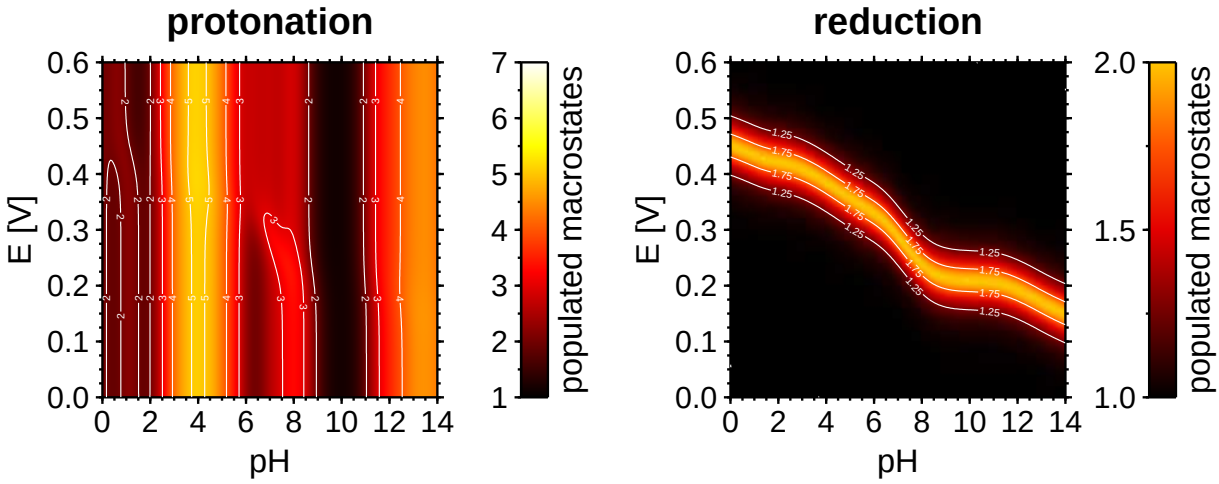

Figure S2: The number of effectively populated macroscopic protonation and reduction states as functions of the pH value and reduction potential of the solution. The number of macrostates effectively populated in equilibrium is given by $\tilde{\Omega} = \left(\sum_{a=1}^{\mathfrak{N}^{\mathrm{macro}}} p_a^2 \right)^{-1}$, where p_a is the equilibrium probability of macrostate a and the sum runs over all $\mathfrak{N}^{\mathrm{macro}}$ macrostates.[3] The number of effectively populated macrostates is color coded (see color bar) and indicated by the contour values. It can be seen that there is always more than one significantly populated protonation macrostate over the whole space of proton and electron chemical potentials investigated. The number of effectively populated protonation macrostates can be as high as 5(!).

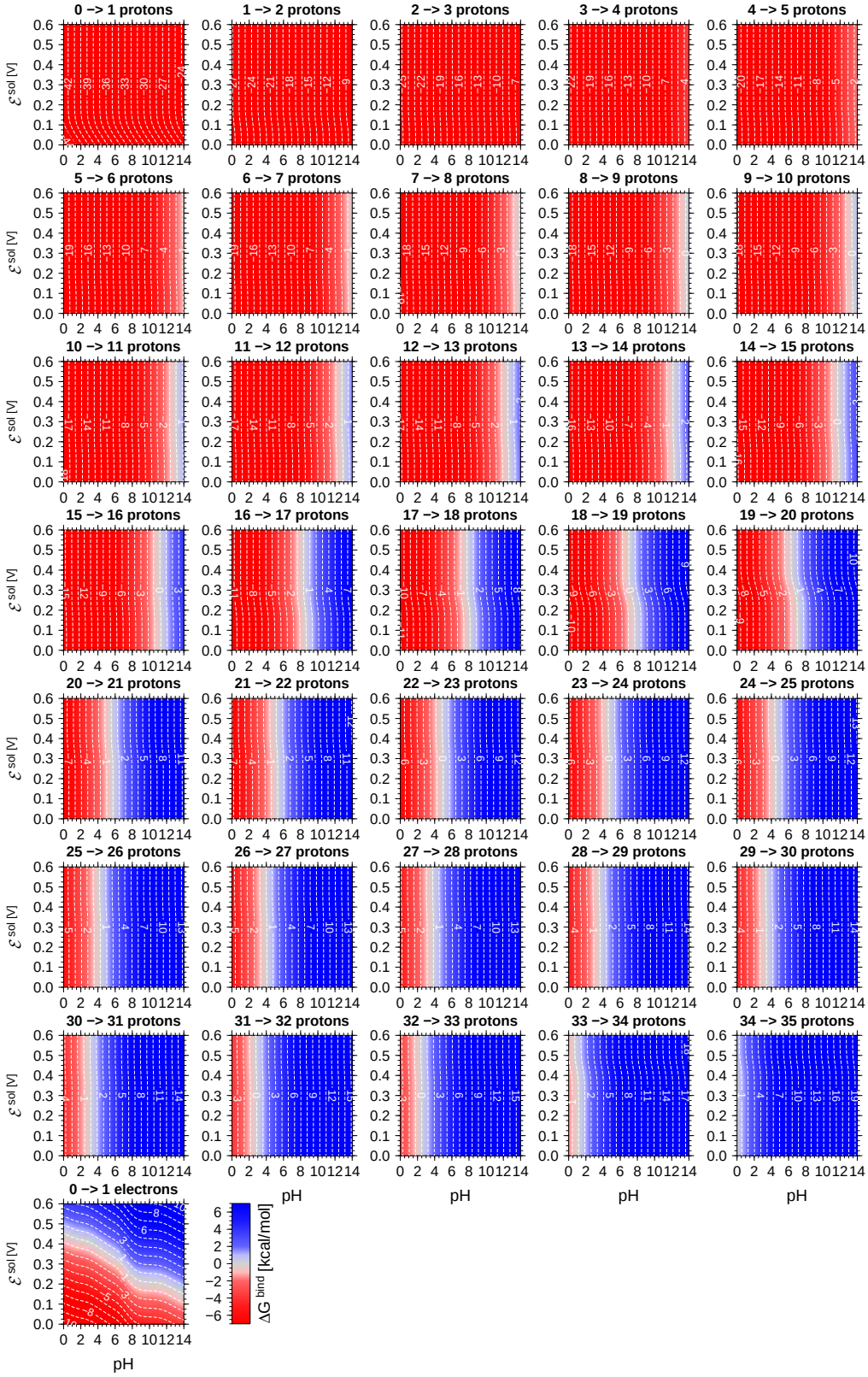

Figure S3: The binding free energies of macroscopic protonation and reduction reactions of PaAz as functions of the pH value and reduction potential of the solution. The number of protons or electrons bound is indicated by the curve labels. The binding free energy is color coded (see color bar). Contour values are given in kcal/mol.

A.2 Binding probabilities of individual sites

Figure S4 shows the spatial position of all sites within the three-dimensional structure of PaAz. Figure S5 shows the protonation probability of all protonatable sites, the reduction probability of the copper center and the occupation probability of the low-pH form of the peptide flip region plotted as functions of the pH value and the reduction potential of the solution. Figure S6 shows plots of the equilibrium occupation probabilities of the forms hpH and lpH in dependence on the pH value and the reduction potential of the solution.

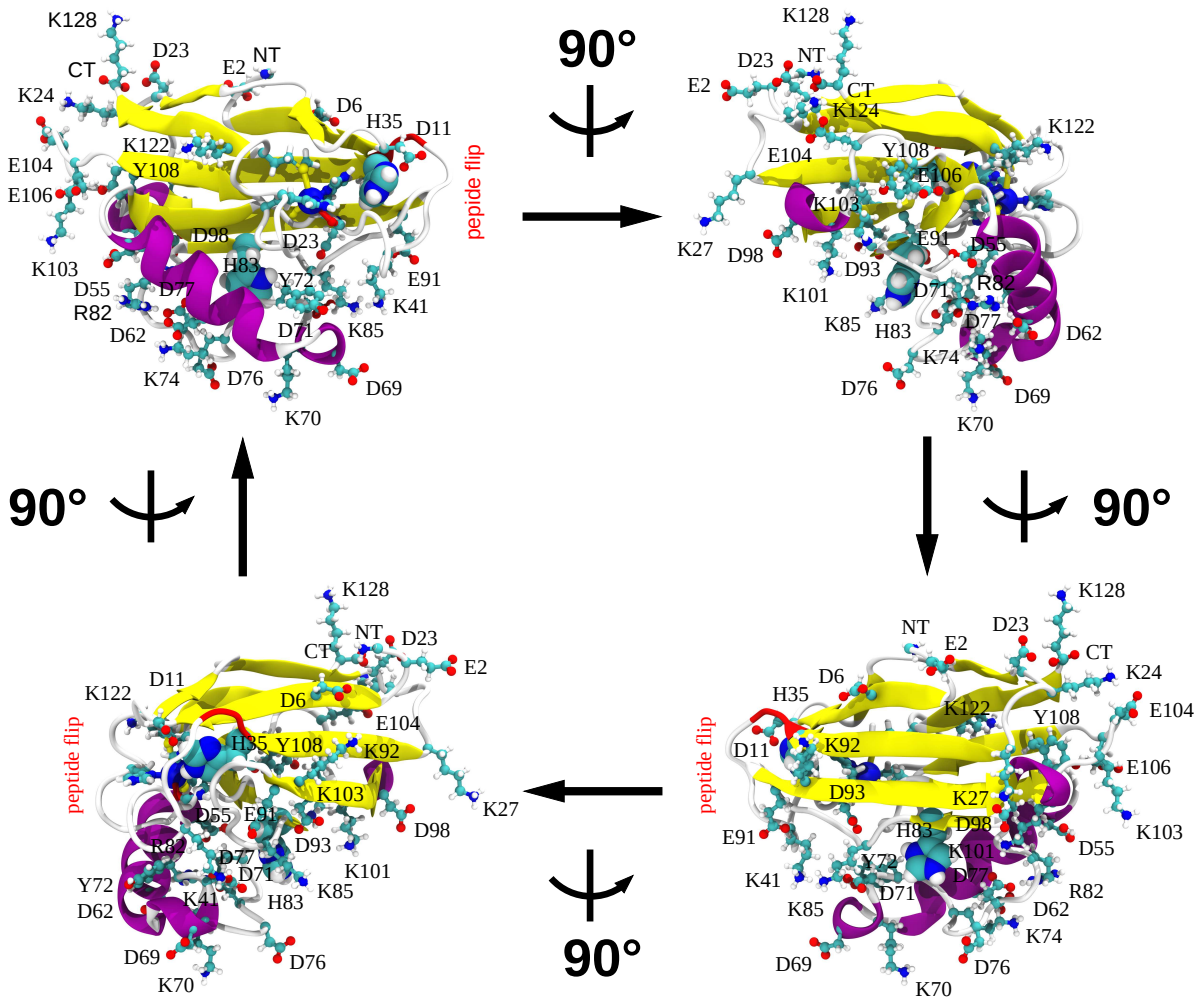

Figure S4: The location of the sites in the three-dimensional structure of PaAz (PDB 4AZU). The protein backbone is shown in cartoon representation. The short red backbone stretch from Pro-36 to Gly-37 indicates the position of the peptide flip region. The upper left perspective shows a frontal view on the hydrophobic patch with the copper center. The structure is successively rotated by 90 degrees to obtain the different views. The copper ion is shown as blue sphere and the coordination sidechains are shown in ball-and-stick representation. His-35 and His-83 are shown in space-filling representation. The sidechains of all other protonatable sites are shown in ball-and-stick representation. The protonatable sites are indicated by labels using one-letter amino acid codes. The labels NT and CT indicate the N-terminus and the C-terminus, respectively.

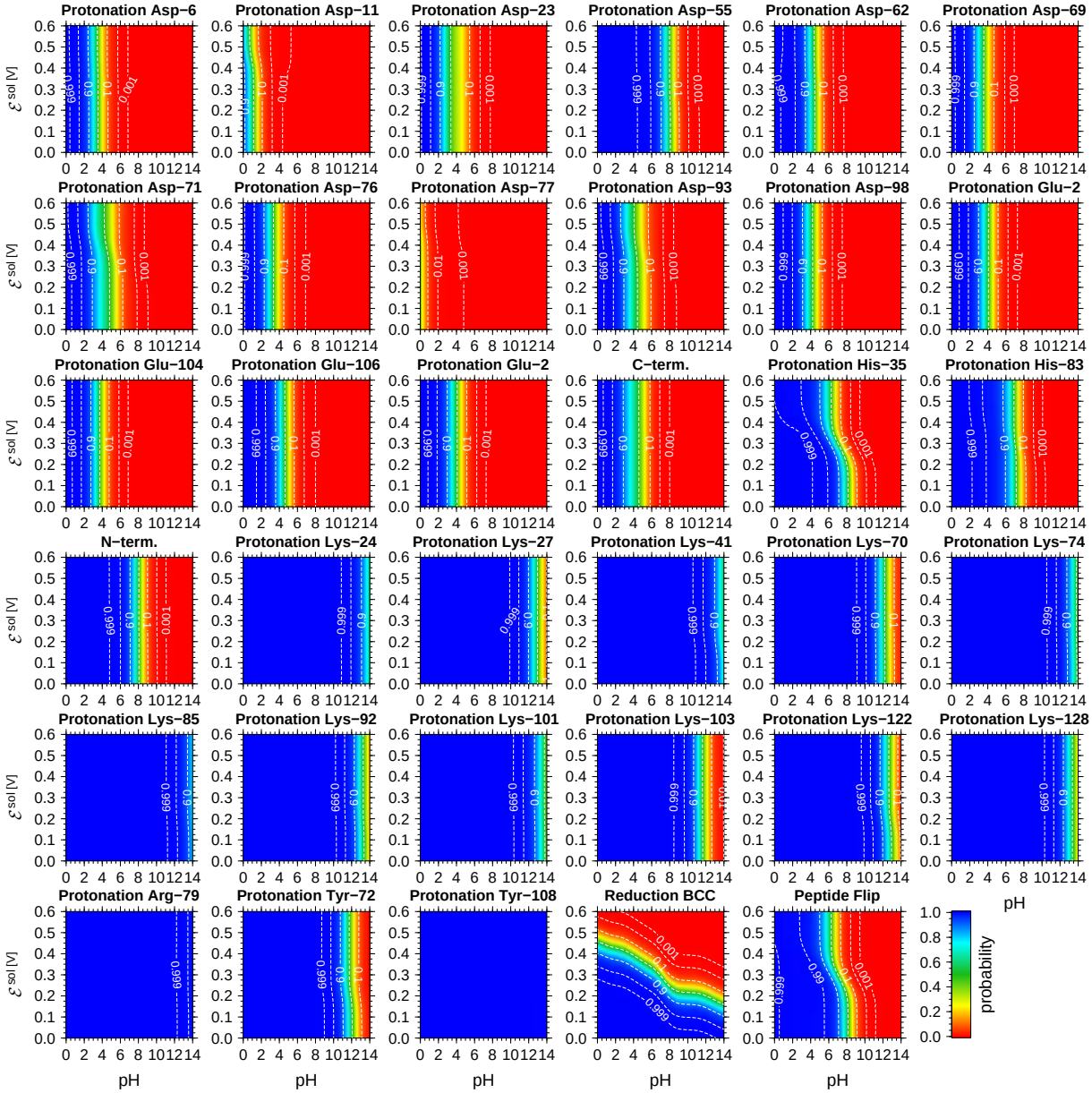

Figure S5: The occupation probabilities of the final state of reactions in PaAz as functions of the pH value and reduction potential of the solution. The reactions are indicated by the curve labels. The probability is color coded (see color bar) and indicated by contour values.

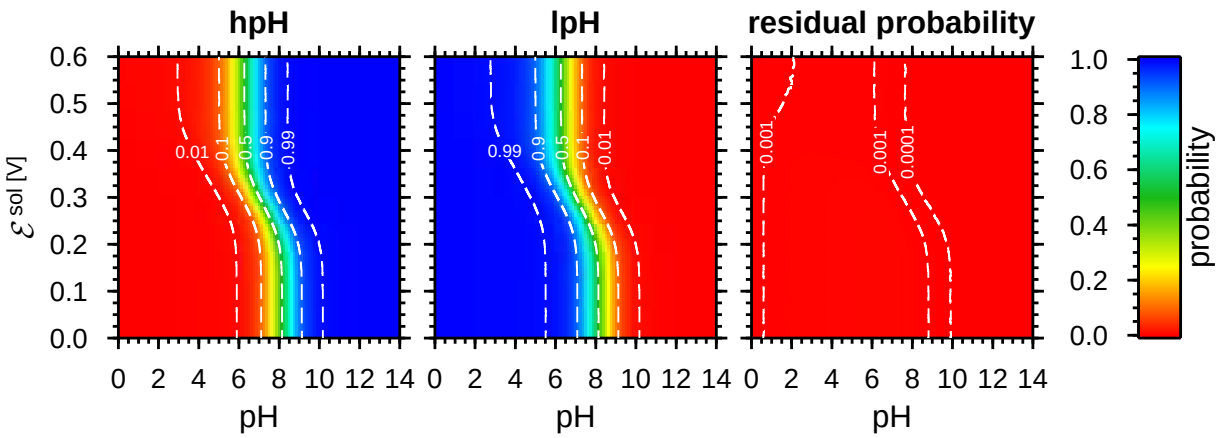

Figure S6: Probability of the low-pH form (lpH) and the high-pH form (hpH). hpH: peptide flip region in the high-pH form and His-35 deprotonated.[4,5] lpH: peptide flip region in the low-pH form and His-35 protonated.[4,5] residual: probability of states other than hpH and lpH, residual = 1 - p(lpH) -p(hpH). Probabilities are color coded (see color bar) and indicated by the contour values. It can be seen that PaAz occupies almost exclusively either the state lpH or the state hpH, indicating the the strong coupling between the peptide flip and the protonation of His-35.

A.3 Reaction free energies for reactions of individual sites

Figure S7 shows the reaction free energies of all reactions of individual sites considered plotted as functions of the pH value and the reduction potential of the solution. Figure S8 shows the protonation free energies and the free energy difference for the peptide flip in terms of thermodynamically defined Henderson-Hasselbalch pK_{a} values[6,7,1] in dependence on the pH value and the reduction potential of the solution. Figure S9 shows the thermodynamically defined Nernst reduction potential[6,1] of the copper center plotted in terms of a in dependence on the pH value and the reduction potential of the solution. The reduction potentials are plotted for the unconstrained system, the system constrained to the low-pH form and the system constrained to the high-pH form as well as the difference in the reduction potential between the two constrained systems.

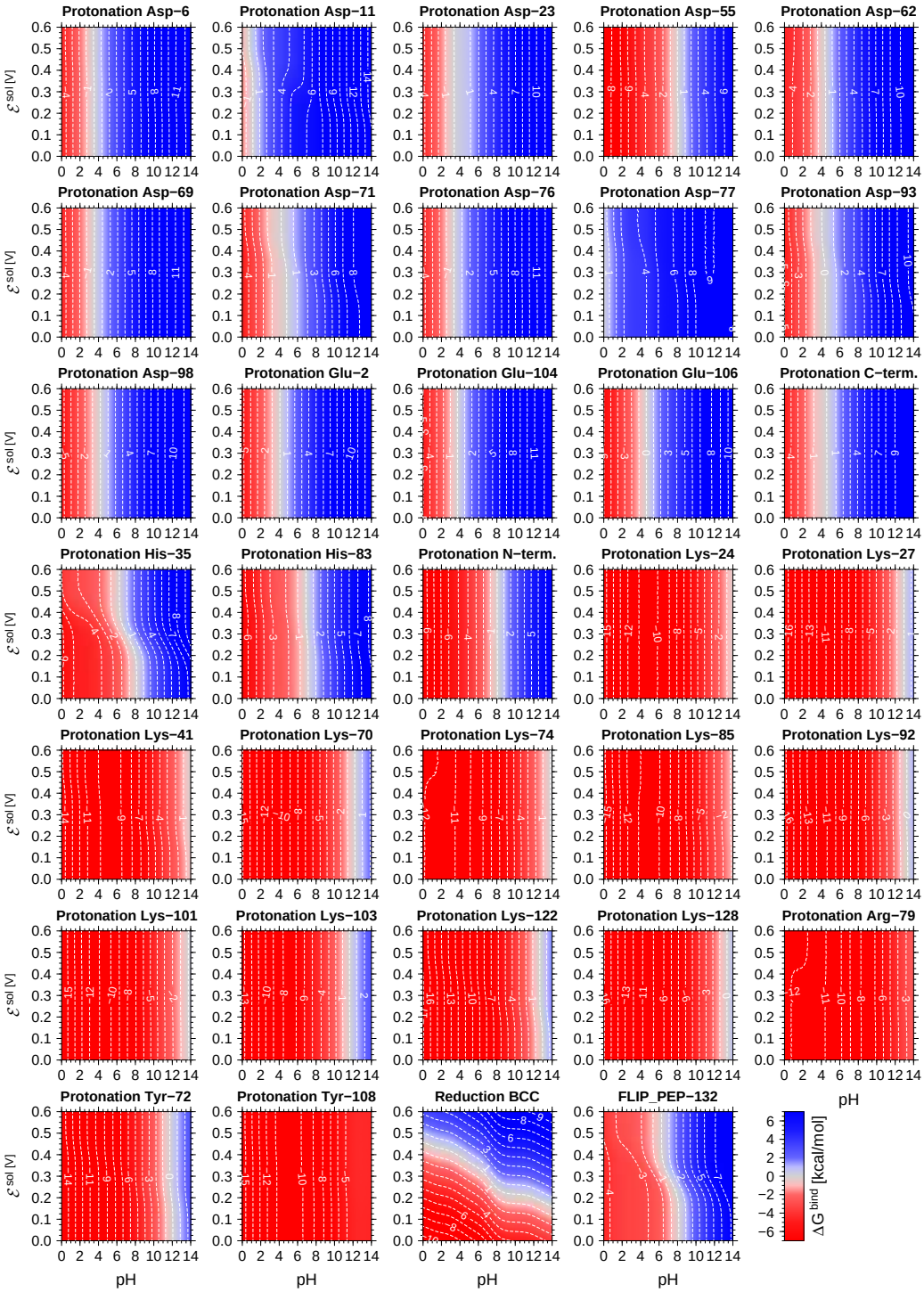

Figure S7: The reaction free energy for reactions of PaAz as functions of the pH value and reduction potential of the solution. The reactions are indicated by the curve labels. The reaction free energy is color coded (see color bar) and indicated by the contour values in kcal/mol. It can also be seen that there are many residues with a weak but significant dependency of the protonation free energy on the reduction potential of the solution. This is more clearly seen then expressing the protonation free energy in terms of the Henderson-Hasselbalch pK_a value (see Figure S8). His-35 is the residue whose protonation free energy shows the greatest dependency on the reduction potential of the solution.

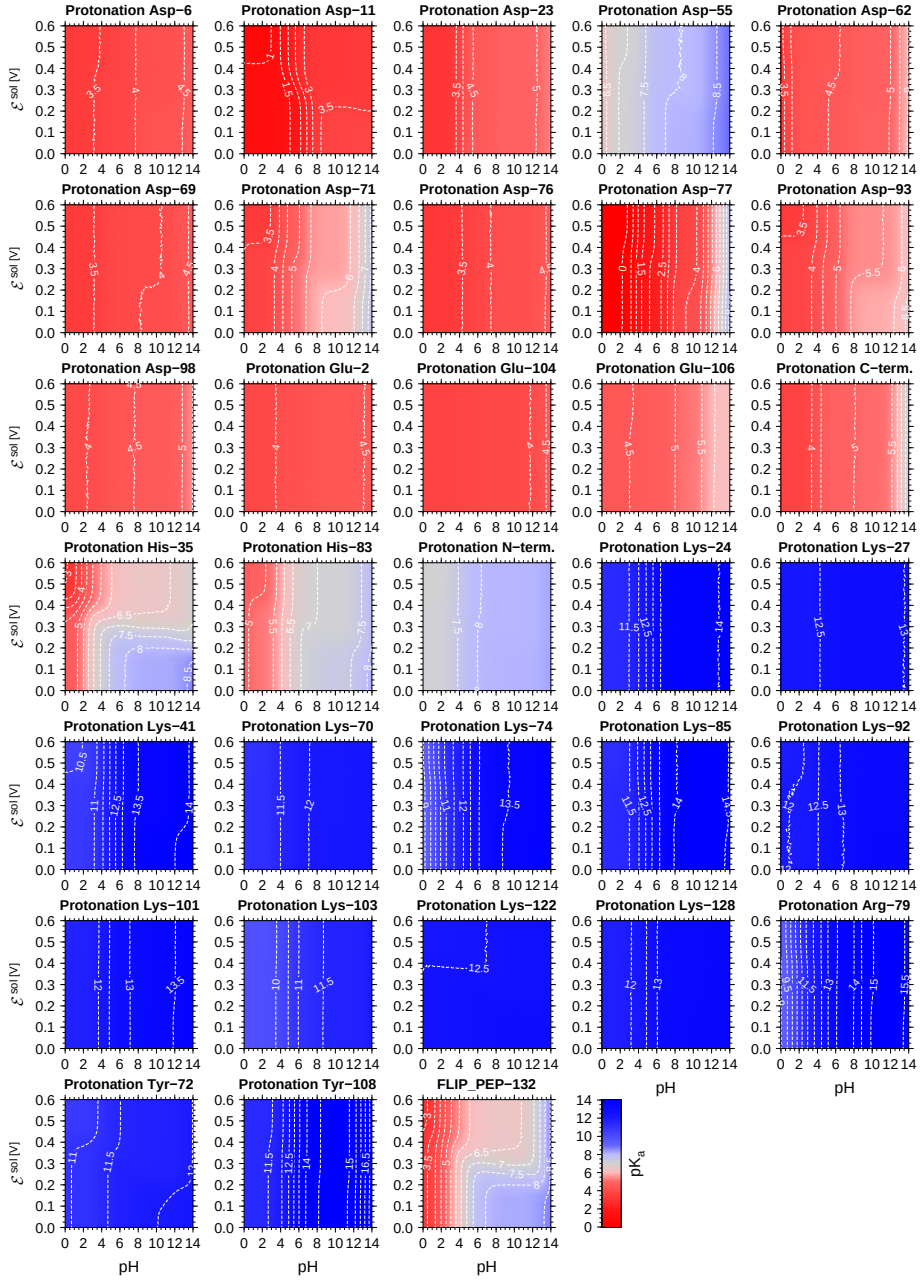

Figure S8: The Henderson-Hasselbalch pK_a values for protonation reactions in PaAz as functions of the pH value and reduction potential of the solution. The reactions are indicated by the curve labels. The Henderson-Hasselbalch pK_a value is given by $\mathrm{p}K_a = \mathrm{pH} - \beta\Delta G^{\mathrm{prot}}/\ln 10$[6,7] and $\mathcal{E} = \mathcal{E}^{\mathrm{sol}} - \Delta G^{\mathrm{red}}/\mathrm{F}$.[6] The p$K_a$ value is color coded (see color bar) and indicated by the contour values. The curve for the peptide flip exhibits an apparent pK_a value that is over wide ranges equal to that of His-35. This indicates a tight coupling between the protonation of His-35 and the peptide flip. It can also be seen that there are many residues with a weak but significant dependency of the pK_a value on the reduction potential of the solution. Among those residues, His-83 is the most notable, because it titrates in the neutral range of the pH value. His-35 is the residue whose pK_a value shows the greatest dependency on the reduction potential of the solution. Furthermore it can be seen that almost all protonatable sites have a pH-dependent pK_a value.

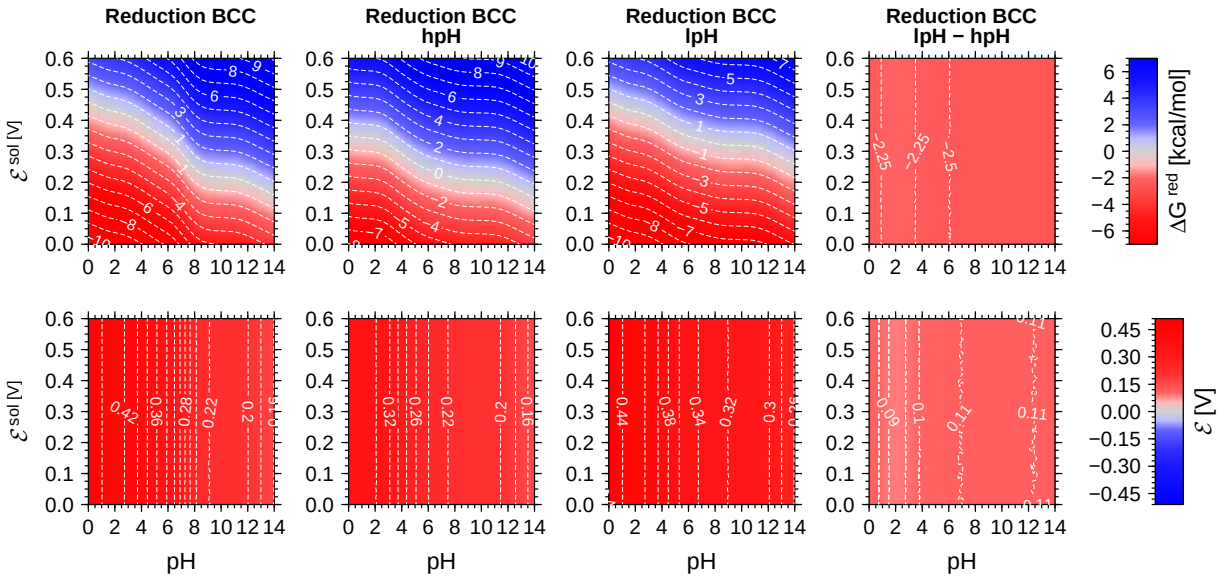

Figure S9: The reduction free energy and the Nernst reduction potential of the copper center as functions of the pH value and reduction potential of the solution. The Nernst reduction potential is given by $\mathcal{E} = \mathcal{E}^{\mathrm{sol}} - \Delta G^{\mathrm{red}}/\mathrm{F}$.[6] The reduction free energy and the reduction potential are color coded (see color bars) and indicated by the contour values in kcal/mol and V, respectively. The reduction reactions of PaAz are indicated by the curve labels. For the left column, the high-pH form (hpH) and the low-pH form (lpH) are populated according to the equilibrium distribution. For the middle columns PaAz was restricted to either the high-pH form (hpH) or the low-pH form (lpH). hpH: peptide flip region in the high-pH form and His-35 deprotonated.[4,5] lpH: peptide flip region in the low-pH form and His-35 protonated.[4,5] The last column shows the shift of the reduction potential that accompanies the transformation of PaAz from the high-pH form to the low-pH form. It can be seen that the shift of the reduction potential is almost constant ($\approx$ 100 mV) over the whole range of pH values investigated.

A.4 Cooperativity free energies between reactions of individual sites

Figures S10 to S12 show the numeric cooperativity free energies from Figure 6 of the main text and the spatial distances of the respective sites involved. Figure S13 shows the cooperativity free energies between the reduction of the copper center and all other reactions of individual sites considered and the cooperativity free energy between the protonation of His-35 and the conformational change of the peptide flip region plotted as functions of the pH value and the reduction potential of the solution. Figure S14 shows the covariance between the final states of all pairs of reactions of individual sites considered plotted as functions of the pH value and the reduction potential of the solution.

We showed in the main text, that apart from His-35 and His-83 many other residues contribute in minor fashion to cooperativity of protonation and reduction (see Figure 6 of the main text, Figs. S10 to S12 and Figure S13). The cooperativity free energies make these minor contributions visible as can be seen from Figure 6. The covariance as cooperativity measure is not very sensitive to such weak couplings and thus fails to reliably indicate weak cooperativity (Figure S14). Furthermore, also the covariance between states of strongly coupled sites is only visible in regions of the chemical potential space in which the events actually and frequently occur in equilibrium. This property of the covariance manifests itself in a coincidence of the regions of chemical potential space with significantly non-zero magnitudes of the covariance and the regions in which the initial and the final states of the involved reactions occurr with probabilities that differ significantly from 0 and 1. The coincidence of these regions is evident from comparison of the covariance plots in Figure S14 and of the corresponding probability plots in Figure S5. In contrast, the cooperativity free energy reliably indicates and quantifies both weak and strong cooperativity for the whole range of ligand chemical potentials as can be seen from Figure S13.

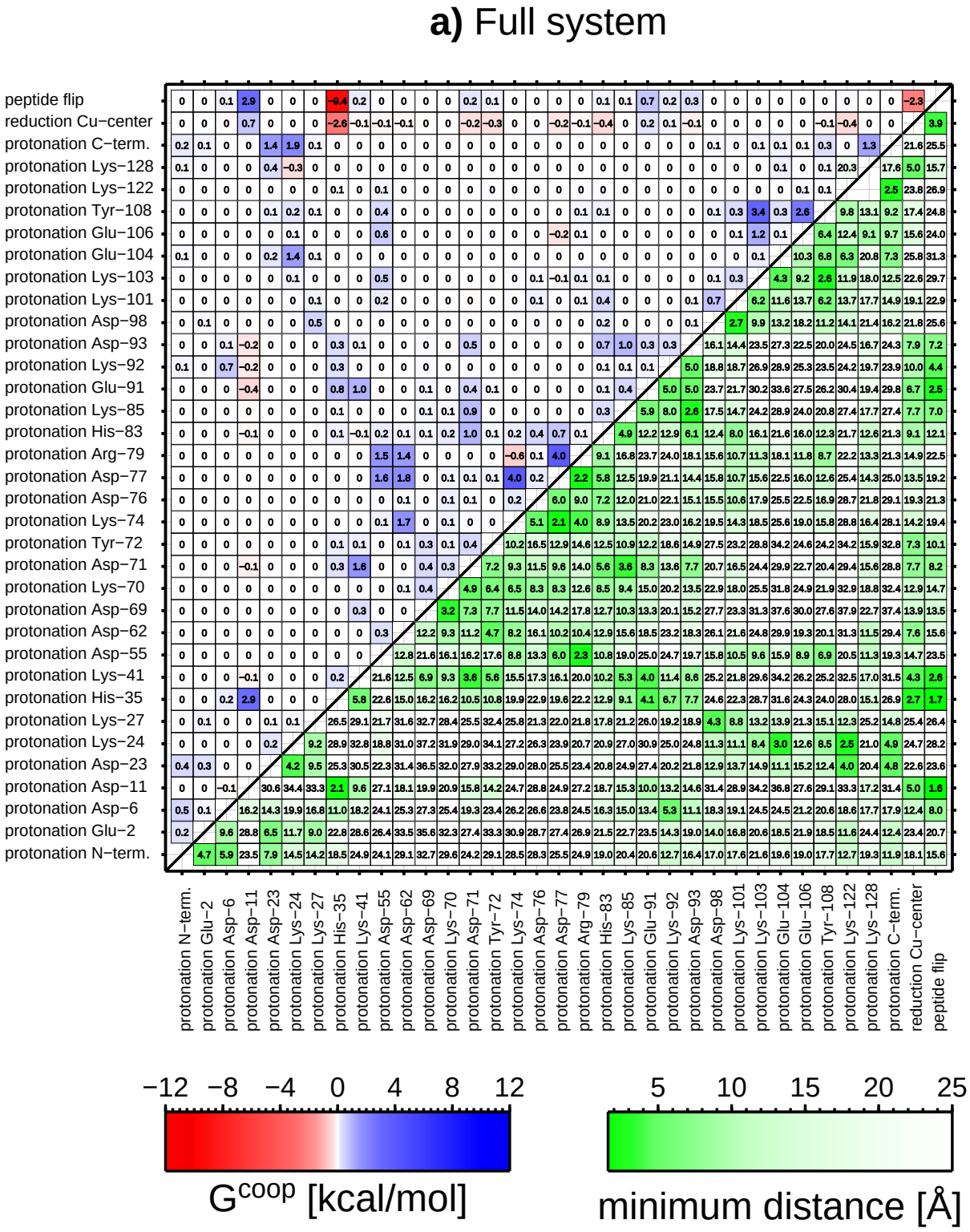

Figure S10: Spatial distances and pairwise cooperativity free energies between reactions of sites in PaAz. The reactions are indicated by the labels on the plot axes. The numbers in the upper left triangel contain the pairwise cooperativity free energies in kcal/mol. The numbers in the lower right triangel contain the minimum spatial distances between the involved sites (see Figure S4 for positions of sites within the structure of PaAz). The numbers in the upper left triangle are underlayed with boxes that are colored according to the magnitude of the cooperativity free energy between the pair of reactions (see color bar). The numbers in the lower right triangle are underlayed with boxes that are colored according to the minimum spatial distance between the pair of sites undergoing the reactions (see color bar).

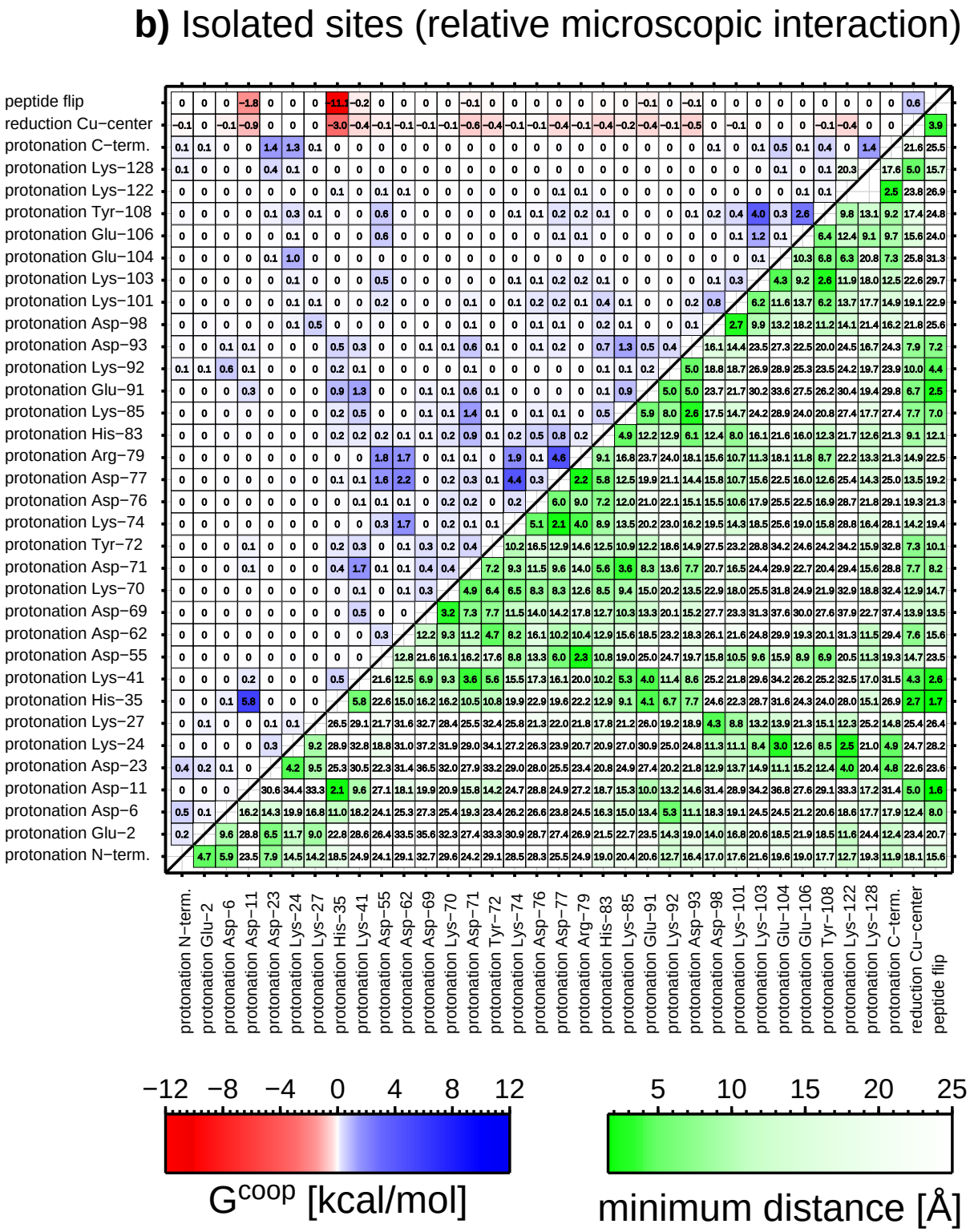

Figure S11: Continued from Figure S10. See caption of Figure S10 for explanation.

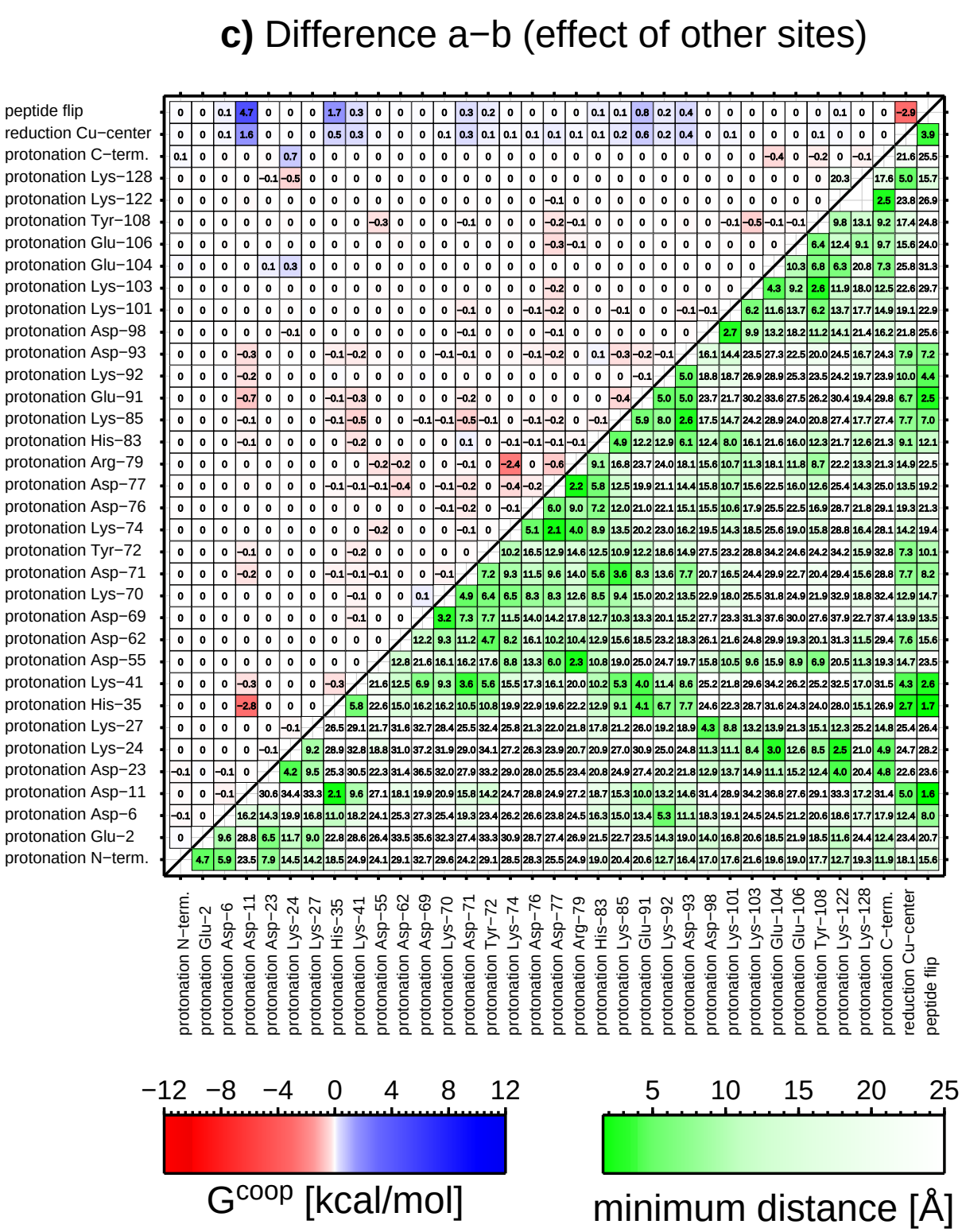

Figure S12: Continued from Figure S11. See caption of Figure S10 for explanation.

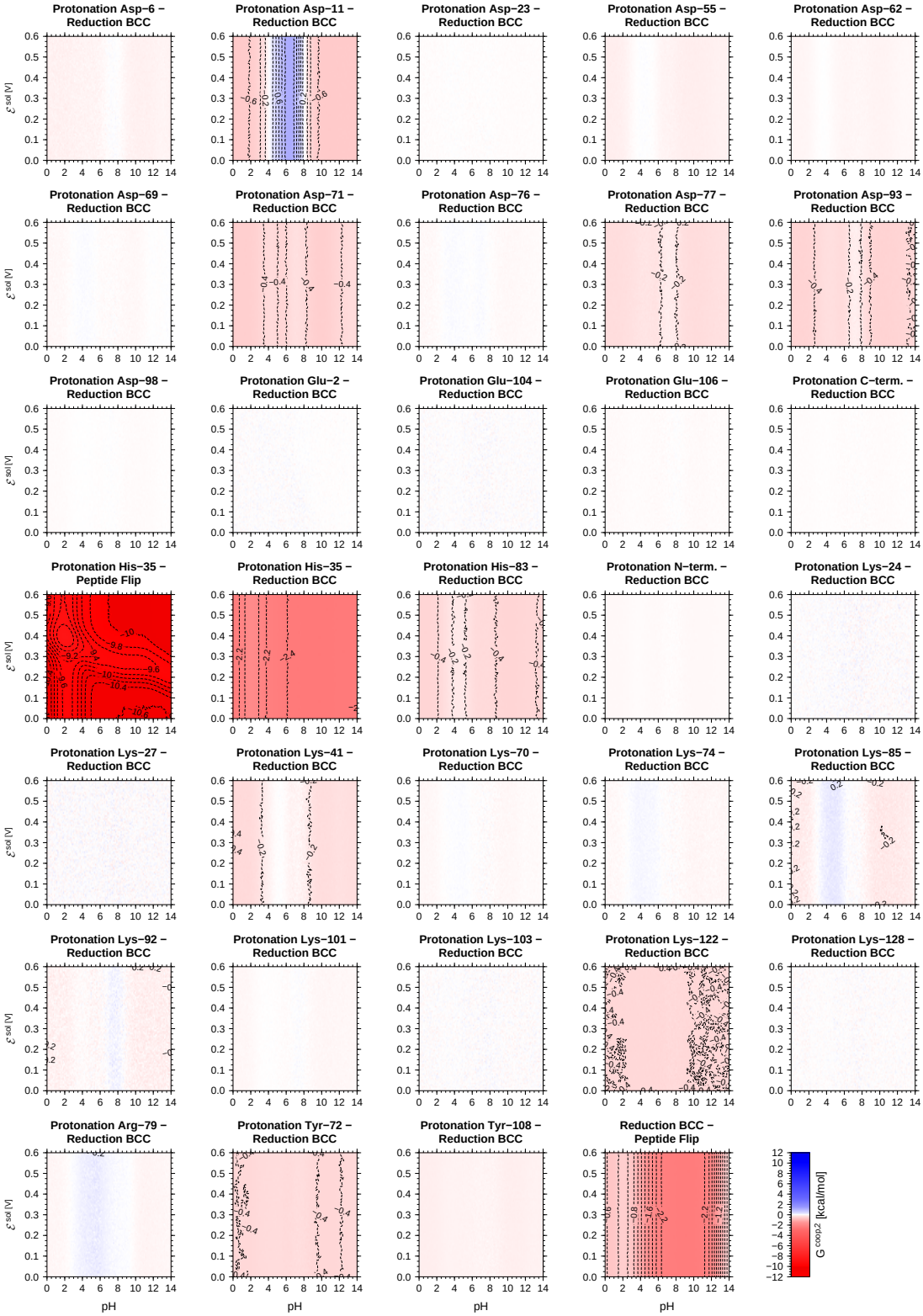

Figure S13: The pairwise cooperativity free energy between reactions in PaAz as functions of the pH value and reduction potential of the solution. Only pairs of reactions that involve the reduction of the copper center or the transition between the high-pH form and the low-pH form are shown. The reactions are indicated by the curve labels. The cooperativity free energy is color coded (see color bar). Contour values are given in kcal/mol.

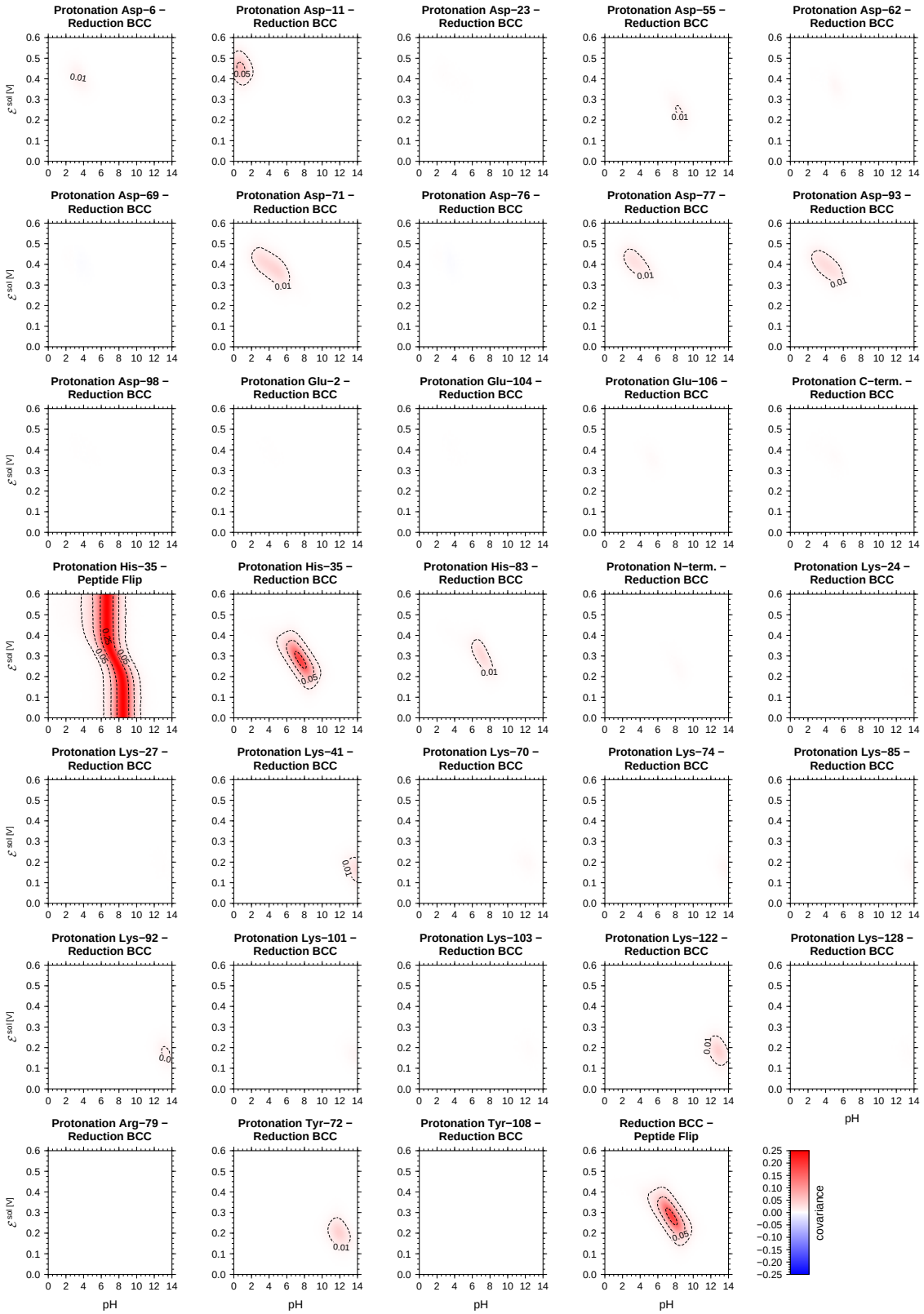

Figure S14: The covariance between the occupancys of the final states for pairs of reactions in PaAz as functions of the pH value and reduction potential of the solution. The reactions are indicated by the curve labels. The covariance is color coded (see color bar) and indicated by contour values.

A.5 Electrostatic surface potential of PaAz

Figure S15 shows the electrostatic potential distribution on the surface of PaAz for different states of PaAz, regarding the reduction of the copper center and the protonation state His-35 which is tightly coupled to the conformational change of the peptide flip region. It can be seen that the prominent negative potential of the His-35 patch for the high-pH form in both reduction states is neutralized in the respective low-pH form. The involvement of the His-35 patch in electron transfer reactions with other proteins was proposed before but later no longer considered due to experiments that confirmed electron transfer (ET) mediation by the hydrophobic patch.[11,12,13] The close proximity of the two patches, however, seems to imply that both patches can play a role in the association with ET partners. Interestingly, the electron self exchange rate of the PaAz mutant M44K was found to be pH-dependent while the corresponding rate of the wildtype PaAz was independent of pH.[11] The residue 44 is located close to the center of the hydrophobic patch.

It is well known that many small cytochrome *c* type, cytochromes possess positively charged lysine residues in close proximity to their hydrophobic patch. These residues could interact favorably with the complementary negative electrostatic potential of the His-35 patch of PaAz in the state high-pH form. This favorable electrostatic interaction would be disrupted if PaAz changes to the low-pH form. The importance of electrostatic interactions in the ET reaction between PaAz and horse heart cytochrome *c* has been demonstrated experimentally.[13]

Studies of covalently linked azurin dimers demonstrated the importance of a close interaction of the hydrophobic patches of the two monomers for efficient ET.[14,15,16] The ET rate was reduced dramatically if a too short linker was used that did not allow the dimer to adopt the most favorable configuration. Cytochrome c_{551} was suspected as one of the physiological ET partners of PaAz in *P. aeruginosa*.[17] A docking study of the complex between PaAz and cytochrome c_{551} of *P. aeruginosa* shows a configuration in which the hydrophobic patches of the partners are tilted away from one another.[18] This is best seen in a picture of the docking model shown in figure 1 of reference 19. The resulting rather large distances between the redox centers seem not to be optimal for efficient ET. The authors 18 do not comment on protonation states chosen for the titratable residues of PaAz, but the low-pH structure (PDB code 4AZU) was used to prepare the structure used in the simulations. If it is the case that PaAz was in the low-pH form during their calculations, our hypothesis about the role of the His-35 patch in the interaction with ET partners would be supported by the model. That is the low-pH form would be the ET-incompetent form, while the high-pH form would be the ET-competent form that permits association of PaAz and its ET partner. The relevant difference for ET between the two forms is the electrostatic potential of PaAz at the His-35 patch. It would be interesting to see whether a repetition of the docking procedure with PaAz in the high-pH form would lead to a docking model with a closer distance of the redox centers.

Experimental work showed that while the ET reactions of PaAz show specificity to-

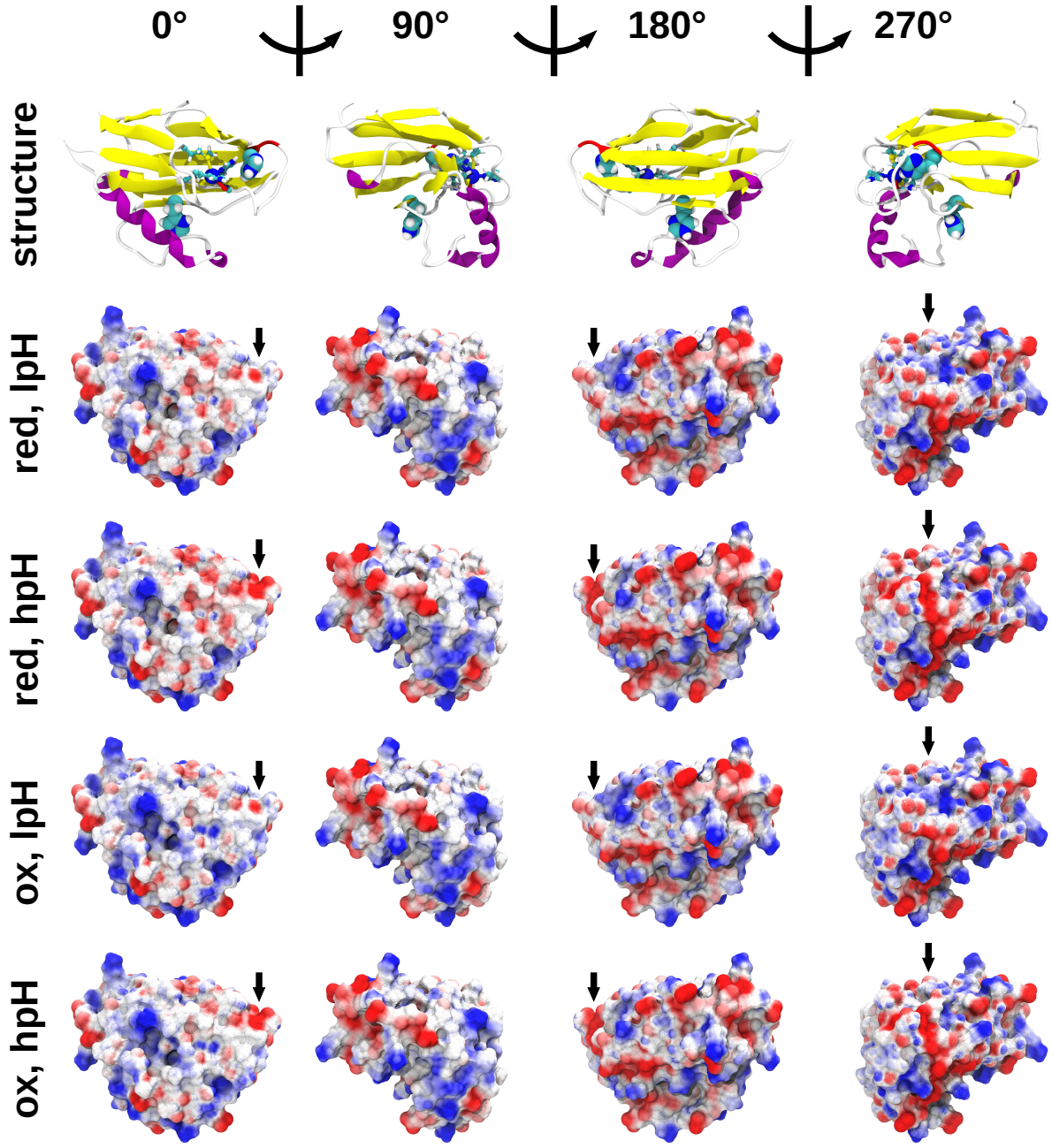

Figure S15: Electrostatic potential distribution on the solvent accessible surface of PaAz for different states at pH = 7.0. The top row shows the structure of PaAz in the same views for orientation. The backbone of Pro-36 and Gly-37 between which the peptide flip occurs is colored red. His-35, His-83 and the copper center are highlighted (cf. Figure 1). The subsequent rows show the electrostatic potential distributions for the forms of PaAz indicated on the left. ox : copper center oxidized, red: copper center reduced, hpH: peptide flip region in the high pH form and His-35 deprotonated,[4,5] lpH: peptide flip region in the low pH form and His-35 protonated.[4,5] The potential is plotted for different viewing angles in steps of 90°. The color scale for the electrostatic potential reaches from red at −77 mV to blue at +77 mV (+/-3 $k_B T/e_\circ$). The leftmost column shows a frontal view on the hydrophobic patch above the copper center that constitutes the the interaction interface with electron transfer partners. The arrows at the plots indicate a region of variable electrostatic potential at the right rim of the hydrophobic patch above the peptide flip region (best seen in the rightmost column). This region is termed His-35 patch and was suspected earlier to be involved in ET reactions of PaAz. It can be seen that the prominent negative potential of the His-35 patch in the form hpH is neutralized in the respective form lpH for oxidized and reduced PaAz. The structures of the states were constructed by setting all sites to their most highly populated instances. There are no significant conformational differences between the states apart from those in the peptide flip region. The net formal charges of the states are ox, hpH : 0; ox, lpH : 1; red, hpH : −1 and red, lpH : 0. The electrostatic potentials and solvent accessible surfaces were computed with our in-house version[8] of the MEAD package.[9,10]

wards cytochrome c_{551} from *P. aeruginosa*, horse heart cytochrome *c* and artificial ET partners can react with PaAz albeit at lower reaction rates.[17] In the same study, it was found that the ET rate between PaAz and cytochrome c_{551} from *P. aeruginosa* does not depend much on the pH value of the solution. This result stands in contradiction to the view that the low-pH form and the high-pH form are strictly ET inactive and active, respectively.[20] ET complexes are often loosely bound and can exhibit considerable configurational variability in the mutual orientation and distance of the redox partners.[21,22,23,24] This is true for the ET productive complex and even more so for the encounter complex that precedes the productive complex during the association of the ET partners.[25] Thus, it would also be interesting to study ET complexes of PaAz in the high and low-pH forms experimentally with NMR methods and theoretically with Monte Carlo methods or Brownian dynamics. One might ask whether the switch between the high-pH and low-pH forms redirects PaAz towards other ET partners in the physiological context instead of shutting down its electron transport function between an electron donor and an electron acceptor completely. *P. aeruginosa* possesses a variety of different bioenergetic pathways. It is conceivable that the pH-dependent equilibrium of PaAz could serve in balancing the flow of electrons between different bioenergetic pathways in the bacterium. This balancing could result from altering the specificity towards different potential ET partners as a result of the altered electrostatic potential of PaAz (see Figure S15).

PaAz has been found to interact with the eukaryotic tumor suppressor protein p53[26] and to protect it from degradation in the cell.[27] It has been speculated that the interaction of PaAz and p53 involves lysine residues of the DNA-binding domain of p53.[28,27] These lysine residues could otherwise be ubiquitinated by the eukaryotic protein Mdm2 leading to degradation of p53. The protection of p53 from degradation by PaAz could thus be based on blocking access of Mdm2 to these lysine residues.[27] Alternative binding modes of PaAz and p53 involving the N-terminal[29] or C-terminal[29,30] domains have also been suggested. In the rightmost column of Figure S15, an elongated region of negative electrostatic potential including the His-35 patch can be seen at the rim of the hydrophobic patch of PaAz in the high-pH form. It is tempting to ask, whether this region mimics the negatively charged DNA backbone in the interaction of PaAz with the DNA binding moieties of p53.

B Parameters

Table S2 lists the model energies of all considered redox and protonation forms of the sites in PaAz. Table S3 lists the atomic partial charges of the oxidized and reduced forms of the copper center. Table S4 lists the atomic partial charges of the protonated and deprotonated forms of the cysteine sidechain. Table S5 lists the atomic partial charges of the protonated and deprotonated forms of the lysine sidechain. Table S6 lists the atomic partial charges of the protonated form and the five tautomers of the deprotonated form of the arginine sidechain.

Site	pK_a^{macro}	Reference	Microscopic form	Intrinsic energy in kcal/mol
α-carboxyl group	3.8	31	protonated at OT1 (syn)	0.0
			protonated at OT1 (anti)	2.0
			protonated at OT2 (syn)	0.0
			protonated at OT2 (anti)	2.0
			deprotonated	4.7
α-amino group	7.5	31	protonated	0.0
			deprotonated (HT1)	10.9
			deprotonated (HT2)	10.9
			deprotonated (HT3)	10.9
Aspartate	4.0	31	protonated at OD1 (syn)	0.0
			protonated at OD1 (anti)	2.0
			protonated at OD2 (syn)	0.0
			protonated at OD2 (anti)	2.0
			deprotonated	5.0
Glutamate	4.4	31	protonated at OE1 (syn)	0.0
			protonated at OE1 (anti)	2.0
			protonated at OE2 (syn)	0.0
			protonated at OE2 (anti)	2.0
			deprotonated	5.6
Tyrosine	9.6	31	protonated (rotamer 1)	0.0
			protonated (rotamer 2)	0.0
			protonated (rotamer 3)	0.0
			deprotonated	12.8
Cys	8.6	32	protonated (rotamer 1)	0.0
			protonated (rotamer 2)	0.0
			protonated (rotamer 3)	0.0
			deprotonated	11.0
His	7.0 ($pK_{a,1}$)[a]	33	doubly-protonated	0.0
			singly protonated at NE1	9.6
	6.6 ($pK_{a,1}$)[b]	33	singly protonated at NE2	9.0
	14.0 ($pK_{a,2}$)	34	fully deprotonated	27.9
Lysine	10.4	31	protonated	0.0
			deprotonated (HZ1)	14.8
			deprotonated (HZ2)	14.8
			deprotonated (HZ3)	14.8
Arginine	12.0	31	protonated	0.0
			deprotonated (HE)	18.8
			deprotonated (HH11)	17.7
			deprotonated (HH12)	19.3
			deprotonated (HH21)	16.0
			deprotonated (HH22)	16.7
Site	$\mathcal{E}^\circ$	Reference	Microscopic form	Intrinsic energy in kcal/mol
copper center	278 mV[c]	35	oxidized	13.3
			reduced	0.0

Table S2: Intrinsic model energies for model compounds of sites in different reduction or protonation forms. Atom names follow the CHARMM nomenclature. All pK_a^{macro} values measured in water. All model energies referenced to water. [a] Model compound methylated at ND1. [b] Model compound methylated at NE2. [c] In azurin from *Alcaligenes denitrificans*.

Residue	Atom	Charge in $e_\circ$	
		Oxidized	Reduced
Gly-45	C	0.477159	0.424549
Gly-45	O	-0.451201	-0.421814
His-46	N	-0.688421	-0.728569
His-46	HN	0.386646	0.369876
His-46	CA	0.288733	0.346013
His-46	HA	0.024656	0.033960
His-46	CB	0.243345	0.257299
His-46	HB1	-0.014586	-0.056869
His-46	HB2	-0.026649	-0.010634
His-46	ND1	-0.504067	-0.490114
His-46	CG	-0.003855	0.002903
His-46	CE1	0.306939	0.330370
His-46	HE1	0.114437	0.117549
His-46	NE2	-0.567731	-0.592510
His-46	HE2	0.464982	0.445365
His-46	CD2	-0.131410	-0.138390
His-46	HD2	0.242737	0.216322
Cys-112	CB	-0.333727	-0.229600
Cys-112	HB1	-0.013379	-0.525655
Cys-112	HB2	0.151521	0.101262
Cys-112	SG	0.164515	0.086042
His-117	CB	0.298419	0.280516
His-117	HB1	0.001535	0.008721
His-117	HB2	-0.091187	-0.071466
His-117	ND1	-0.503482	-0.482917
His-117	CG	-0.066573	-0.066438
His-117	CE1	0.382218	0.367905
His-117	HE1	0.175135	0.159935
His-117	NE2	-0.527785	-0.552523
His-117	HE2	0.426319	0.394229
His-117	CD2	-0.132128	-0.142083
His-117	HD2	0.270944	0.236532
Met-121	CB	0.153011	0.126632
Met-121	HB1	-0.030832	-0.023961
Met-121	HB2	-0.069075	-0.064125
Met-121	CG	0.143390	0.128324
Met-121	HG1	-0.015501	-0.043709
Met-121	HG2	0.003573	-0.004790
Met-121	SD	-0.120981	-0.238312
Met-121	CE	0.045691	0.096689
Met-121	HE1	0.040869	0.037776
Met-121	HE2	0.066122	0.034959
Met-121	HE3	0.053987	0.016175
Cu	Cu	0.365687	0.264576

Table S3: Atomic partial charges for the reduction forms of the blue copper center.

Atom	Charge in $e_\circ$			
	Protonated			Deprotonated
	Rotamer 1	Rotamer 2	Rotamer 3	
CB	-0.053000	-0.053000	-0.053000	-0.549000
HB1	0.079000	0.079000	0.079000	0.157000
HB2	0.079000	0.079000	0.079000	0.157000
SG	-0.195000	-0.195000	-0.195000	-0.765000
HG1	0.090000			
HG2		0.090000		
HG3			0.090000	

Table S4: Atomic partial charges for the protonation forms of cysteine. Charges of chemically equivalent atoms were averaged.

Atom	Charge in $e_\circ$			
	Protonated	Deprotonated		
		HZ1	HZ2	HZ3
CB	0.248895	0.170819	0.170819	0.170819
HB1	-0.087509	-0.069602	-0.069602	-0.069602
HB2	-0.087509	-0.069602	-0.069602	-0.069602
CG	0.089366	0.017558	0.017558	0.017558
HG1	-0.040668	-0.035420	-0.035420	-0.035420
HG2	-0.040668	-0.035420	-0.035420	-0.035420
CD	0.069675	0.111662	0.111662	0.111662
HD1	-0.007345	-0.038777	-0.038777	-0.038777
HD2	-0.007345	-0.038777	-0.038777	-0.038777
CE	-0.016073	0.372979	0.372979	0.372979
HE1	0.076595	-0.055492	-0.055492	-0.055492
HE2	0.076595	-0.055492	-0.055492	-0.055492
NZ	0.270672	-0.870288	-0.870288	-0.870288
HZ1	0.151773		0.297926	0.297926
HZ2	0.151773	0.297926		0.297926
HZ3	0.151773	0.297926	0.297926	

Table S5: Atomic partial charges for the protonation forms of lysine. Charges of chemically equivalent atoms were averaged.

Atom	Charge in $e_\circ$					
	Protonated	Deprotonated				
		HE	HH11	HH12	HH21	HH22
CB	0.135709	0.006692	-0.029587	-0.029587	-0.029587	-0.029587
HB1	-0.039279	-0.042325	-0.018617	-0.018617	-0.018617	-0.018617
HB2	-0.039279	-0.042325	-0.018617	-0.018617	-0.018617	-0.018617
CG	0.099734	0.102169	0.265452	0.265452	0.265452	0.265452
HG1	-0.013174	-0.034039	-0.083093	-0.083093	-0.083093	-0.083093
HG2	-0.013174	-0.034039	-0.083093	-0.083093	-0.083093	-0.083093
CD	-0.040286	0.784104	0.313235	0.313235	0.313235	0.313235
HD1	0.090910	-0.161848	-0.036989	-0.036989	-0.036989	-0.036989
HD2	0.090910	-0.161848	-0.036989	-0.036989	-0.036989	-0.036989
NE	-0.236304	-0.928518	-0.604232	-0.604232	-0.604232	-0.604232
HE	0.376185		0.329542	0.329542	0.329542	0.329542
CZ	-0.298752	0.691347	0.564502	0.564502	0.564502	0.564502
NH1	-0.054646	-0.762499	-0.887991	-0.887991	-0.696479	-0.696479
HH11	0.249023	0.336407		0.391588	0.315684	0.315684
HH12	0.249023	0.336407	0.391588		0.315684	0.315684
NH2	-0.054646	-0.762499	-0.696479	-0.696479	-0.887991	-0.887991
HH21	0.249023	0.336407	0.315684	0.315684		0.391588
HH22	0.249023	0.336407	0.315684	0.315684	0.391588	

Table S6: Atomic partial charges for the protonation forms of arginine. Charges of chemically equivalent atoms were averaged.

References

[1] Ullmann, R. T; Ullmann, G. M. **2010**. GMCT - Monte Carlo simulation software for macromolecular receptors with multiple ligands, membrane potential and conformational flexibility, submitted for publication.

[2] Süßmann, G. *Z. Naturforsch., A: Phys. Sci.* **1997**, *52a*, 49–52.

[3] Ullmann, R. T; Ullmann, G. M. *J. Phys. Chem. B* **2011**, *115*, 507–521.

[4] Nar, H; Huber, R; Messerschmidt, A; Fillipou, A. C; Barth, M; Jaquinod, M ; van de Kamp, M. *Eur. J. Biochem.* **1992**, *205*, 1123–1129.

[5] Nar, H. **1992** Ph.D. thesis (Technical University of Munich, Munich, Germany).

[6] Ullmann, G. M. *J. Phys. Chem. B* **2000**, *104*, 6293–6301.

[7] Bombarda, E; Ullmann, G. M. *J. Phys. Chem. B* **2010**, *114*, 1994–2003.

[8] Ullmann, R. T; Ullmann, G. M. **2010** . unpublished results.

[9] Bashford, D. **1997** in *Scientific computing in object-oriented parallel environments*, Lecture Notes in Computer Science, eds. Ishikawa, Y; Oldehoeft, R; Reynders, J ; Tholburn, M. (Springer : Berlin / Heidelberg, Gemany) Vol. 1343, pp. 233–240.

[10] Bashford, D. *Frontiers in Bioscience* **2004**, *9*, 1082–1099.

[11] van de Kamp, M; Floris, R; Hali, F. C ; Canters, G. W. *J. Am. Chem. Soc.* **1990**, *112*, 907–908.

[12] van de Kamp, M; Floris, R; Hali, F. C ; Canters, G. W. *Eur. J. Biochem.* **1990**, *194*, 109–118.

[13] Sokerina, E. V; Ullmann, G. M; van Pouderoyen, G; Canters, G. W ; Kostić, N. M. *J. Biol. Inorg. Chem.* **1999**, *4*, 111–121.

[14] van Amsterdam, I. M. C; Ubbink, M; Jeuken, L. J. C; Verbeet, M. P; Einsle, O; Messerschmidt, A ; Canters, G. W. *Chem. Eur. J.* **2001**, *7*, 2398–2406.

[15] van Amsterdam, I. M. C; Ubbink, M; Jeuken, L. J. C; Verbeet, M. P; Einsle, O; Messerschmidt, A ; Canters, G. W. *Nat. Struct. Biol.* **2002**, *9*, 48–52.

[16] van Amsterdam, I. M. C; Ubbink, M ; Canters, G. W. *Inorg. Chimica Acta* **2002**, *331*, 296–392.

[17] Antonini, E; Finazzi-Agrò, A; Avigliano, L; Guerrieri, P; Rotilio, G ; Mondova, B. *J. Biol. Chem.* **1970**, *245*, 4847–4849.

[18] Bizzarri, A. R; Brunori, E; Bonanni, B ; Cannistraro, S. *J. Mol. Recognit.* **2007**, *20*, 122–131.

[19] Bonanni, B; Kamruzzahan, A. S. M; Bizzarri, A. R; Rankl, C; Gruber, H. J; Hinterdorfer, P ; Cannistraro, S. *Biophys. J.* **2005**, *89*, 2783–2791.

[20] Corin, A. F; Bersohn, R ; Cole, P. E. *Biochemistry* **1983**, *22*, 2032–2038.

[21] Ubbink, M. *FEBS Letters* **2009**, *583*, 1060 – 1066.

[22] Ubbink, M. *Photosynth. Res.* **2004**, *81*, 277–287.

[23] Prudêncio, M; Ubbink, M. *J. Mol. Recognit.* **2004**, *17*, 1099–1352.

[24] Crowley, P. B; Carrondo, M. A. *Proteins* **2004**, *55*, 603–612.

[25] Bashir, Q; Volkov, A; Ullmann, G. M ; Ubbink, M. *J. Am. Chem. Soc.* **2010**, *132*, 241–247.

[26] Apiyo, D; Wittung-Stafshede, P. *Biochem. Biophys. Res. Commun.* **2005**, *332*, 965 – 968.

[27] Funari, G; Domenici, F; Nardinocchi, L; Puca, R; d'Orazi, G; Bizzarri, A. R ; Cannistraro, S. *J. Mol. Recognit.* **2010**, *23*, 343–351.

[28] de Grandis, V; Bizzarri, A. R ; Cannistraro, S. *J. Mol. Recognit.* **007**, *20*, 215–226.

[29] Taranta, M; Bizzarri, A. R ; Cannistraro, S. *J. Mol. Recognit.* **2009**, *22*, 215–222.

[30] Xu, C; Zhao, Y ; Zhao, B. *Archives of Biochemistry and Biophysics* **2010**, *503*, 223 – 229.

[31] Nozaki, Y; Tanford, C. *Meth. Enzymol.* **1967**, *11*, 715–734.

[32] Thurlkill, R. L; Grimsley, G. R; Scholtz, J. M ; Pace, C. N. *Prot. Sci.* **2006**, *15*, 1214–1218.

[33] Tanokura, M. *Biochim. Biophys. Acta* **1983**, *742*, 576–585.

[34] Kaim, W; Schwederski, B. **1995** *Bioinorganic Chemistry: Inorganic Elements in the Chemistry of Life.* (New York).

[35] St Clair, C. S; Ellis, W. R. J ; Gray, H. B. *Inorg. Chimica Acta* **1991**, *191*, 149–155.